Biophysical Journal, Volume *112*

Supplemental Information

3D Protein Dynamics in the Cell Nucleus

Anand P. Singh, Rémi Galland, Megan L. Finch-Edmondson, Gianluca Grenci, Jean-Baptiste Sibarita, Vincent Studer, Virgile Viasnoff, and Timothy E. Saunders

Probing dynamic architecture of nuclear proteins in 3D with photo-convertible imaging fluorescence correlation spectroscopy

Anand P. Singh[1,†], Rémi Galland[2,3,†], Megan L. Finch-Edmondson[1,4], Gianluca Grenci[1], Jean-Baptiste Sibarita[2,3], Vincent Studer[2,3], Virgile Viasnoff[1,5,6]*, and Timothy E. Saunders[1,5,7]*

[1]Mechanobiology Institute, National University of Singapore, Singapore

[2]Institut Interdisciplinaire de Neurosciences, University of Bordeaux, France

[3]CNRS UMR 5297, University of Bordeaux, France

[4]Department of Physiology, National University of Singapore, Singapore

[5]Department of Biological Sciences, National University of Singapore, Singapore

[6]CNRS UMI 3639, Singapore

[7]Institute for Molecular and Cell Biology, A*Star, Singapore

[†]These authors contributed equally to this work.

*Co-corresponding authors Virgile.Viasnoff@espci.fr and dbsste@nus.edu.sg

Supplementary Material

Materials and methods

Imaging FCS and data fitting

Imaging FCS analyzes the variation in the time-dependent intensity autocorrelation function (ACF). In imaging FCS, each pixel of the 2D array detectors camera yields fluorescence intensity fluctuations from a small observation volume, over a period of typically ~20-40 sec at high framerate of up to 250-1000 fps. Temporal intensity fluctuations can be used to infer the underlying dynamics (or photo-physical fluorescence fluctuations) of the fluorescently-tagged molecules. The ACF for a fluorescent signal collected over time is given by *G(τ)*

$$G(\tau) = \frac{\langle \delta I(t) \cdot \delta I(t+\tau) \rangle}{\langle I(t) \rangle^2} + G_\infty , \qquad (1)$$

where *G(τ)* is the normalized autocorrelation function, τ the correlation time, $I(t)$ represents the instantaneous fluorescence intensity at time *t*, $\delta I(t)$ the change in fluorescence intensity (deviation from mean value $\delta I(t) = I(t) - \langle I \rangle$), $\langle -- \rangle$ denotes time averaging, and G_∞ is the correlation at long time or the correlation offset value.

To infer dynamic parameters, we fit the measured ACF (Eq. 1) with the prediction from a molecule diffusing in three-dimensions $G_{3D}(\tau)$ (see detailed derivation elsewhere (1)):

$$G_{3D}(\tau) = \frac{1}{N\sqrt{1+\frac{4D\tau}{w_z^2}}} \left[\frac{\frac{\sqrt{4D\tau + w_{xy}^2}}{\sqrt{\pi}.a} \left\{ e^{-\frac{a^2}{4D\tau + w_{xy}^2}} - 1 \right\} + \operatorname{erf}\left(\frac{a}{\sqrt{4D\tau + w_{xy}^2}} \right)}{\operatorname{erf}\left(\frac{a}{w_{xy}} \right) + \frac{w_{xy}}{\sqrt{\pi}.a} \left\{ e^{-\left(\frac{a}{w_{xy}}\right)^2} - 1 \right\}} \right]^2 + G_\infty , \qquad (2)$$

The measurable parameters are the camera pixel size *a* in object space, the lateral, and axial PSF size w_{xy}, w_z,. The variables fitted are the diffusion coefficient *D*, the average particle *N*, and the correlation convergence value G_∞.

Microfabrication wells for creating light sheet and cell holder

Micro-mirroring surfaces were produced in silicon wafer by anisotropic etching in alkaline solution. Micro-wells of 40x40 μm^2 were then created by deep reactive ion etching process through openings in AZ9260 positive tone resist. The silicon wafer with 45° mirroring surfaces and micro-wells were then replicated in a UV-curable and index-matched polymer on clean #1.5H coverslips in a two-step process: (i) replication of the silicon master mold in PDMS; (ii) reproduction of the PDMS imprint on a coverslip by capillary filling and UV-curing of the UV-curable polymer. The plastic chips were then coated with a thin layer of gold by thermal evaporation in a vacuum chamber to make the 45° surfaces reflective. After metallization, a flat PDMS stamp was deposited on top of the mirror to allow filling the gap in between the mirror by a UV-curable polymer layer by capillary filling. Once the polymer cured, the PDMS stamp was removed, and the metal coating outside the mirror was removed

by wet etching. The coverslip was finally sealed in a bottom-free 35 mm plastic dish that allowed easy surface passivation with 0.1% Pluronic solution overnight and cell seeding and culturing. Further details are described in (2).

soSPIM light sheet scanning unit and bead scan PSF characterization

The soSPIM beam steering unit is composed of a cylindrical lens, a tunable lens and a pair of galvanometric mirror. x- and y-axis positioning of the light-sheet in soSPIM are controlled by the galvanometric mirrors conjugated by two relay lenses. Scanning the excitation beam along the mirror long axis (y-axis) creates the light-sheet, and displacing the light-sheet along the mirror short axis (x-axis) changes the light-sheet depth into the sample. As an alternative to scanning the excitation beam, a cylindrical lens can also be used to create a static light-sheet. The positioning of the light-sheet waist on the sample ROI is achieved using a tunable lens (TL) which defocalizes the excitation beam away from the mirror. The focal length of the tunable lens is maintained by a built-in feedback loop system and set to position the thinnest part of the light-sheet at the sample.

The micro-fabricated device containing the cells was placed on the microscope stage and a 60x WI high NA objective was used for imaging. The orientation of the light-sheet relative to the mirror orientation was adjusted by a cylindrical lens rotational mount. The long axis of the mirror for the axial displacement of the light-sheet was determined according to the mirror orientation in the objective field of view. For two different positions of the light-sheet on the mirror, the axial position of the objective was adjusted to superpose the objective focal plane and the light-sheet, and the appropriate defocus strength was adjusted according to the distance of the sample from the micro-mirror. A custom-written MetaMorph plugin ensures the synchronization between the light-sheet displacement along the mirror with the axial position of the objective and the defocus strength by linear regression between these two calibration points.
To estimate the depth of focus and thickness of the light-sheet, the light-sheet, superposed to the objective focal plane, was scanned along the axial direction and the beads imaged with a step-size of 100 nm in the z-axis. The bead images were projected using maximum intensity along the x-axis and the axial dimension measured by Gaussian fitting along the z direction for each bead. The axial dimension of each bead (full width at half maximum) was then recorded according to their position from the 45° mirror. To estimate the width of the static light-sheet created inserting a cylindrical lens into the beam steering unit optical path, the light-sheet was imaged through a fluorescent polymer after reflection on the 45° mirror. The light sheet profile was then extracted and fitted with a Gaussian function to estimate its width (see Fig. S3).

Dendra2-YAP and 3xNLS-Dendra2 stable cell lines

The coding sequences for 3xNLS-Dendra2 and untagged Dendra2 with the stop codon removed were PCR amplified before being cloned into the retroviral expression vector pBABE puro using BamHI and EcoRI restriction sites. The coding sequence for human YAP isoform 1-2α (3) was then C-terminally sub-cloned in-frame with Dendra2 using EcoRI and SalI restriction sites to generate Dendra2-YAP.

Subconfluent HEK293T cells were co-transfected with pBABE puro 3xNLS-Dendra2 or Dendra2-YAP together with the pCL10A-1 packaging construct using TransIT-293 Transfection Reagent according to the manufacturers specifications. After 48h, the viral supernatants were collected, filtered, and mixed with polybrene before being added to subconfluent YAP null MKN28 cells that had been previously generated using CRISPR-Cas9.

After 24h stably-transduced cells were selected using puromycin before cells were used for imaging experiments.

Cell culture and seeding in micro fabricated wells

Stably expressing H2B-eGFP NIH3T3 Dendra2-Pol II U2OS cells were cultured in high glucose Dulbecco's modified eagle media, supplemented with 10% fetal bovine serum, 1% GlutaMAX and 1% penicillin/streptomycin. Stably expressing 3xNLS-Dendra2 and Dendra2-YAP MKN28 cells were cultured in RPMI 1640 media supplemented with 10% fetal bovine serum and 1% penicillin/streptomycin. All cells were maintained in 5% CO_2 at 37°C. The day prior to seeding into 40x40 μm^2 micro-wells, cells were cultured in 35 mm plastic dishes to ensure they reached 70% confluence on the day of seeding. Before seeding, cells were gently washed twice with 1X PBS and trypsinized for 2 mins. After removing the trypsin, cells were immersed in 1 mL of growth media, and allowed to recover for 10 mins in the incubator.

For cell seeding into the micro-wells, around 0.5 million cells were deposited onto the micro-wells and placed in the incubator for 15 mins, allowing the cells to fill the micro-wells by gravity. The density of cells was adjusted to ensure efficient seeding of the wells with one cell in each well. Cells remaining outside wells were removed by rinsing twice with media, and the device was filled with 2 mL of growth media. This seeding step was repeated up to three times to ensure a filling ratio of 60-80% of wells. The cells were then allowed to recover for one to three hours in growth media in the incubator before imaging.

Supplementary Figures

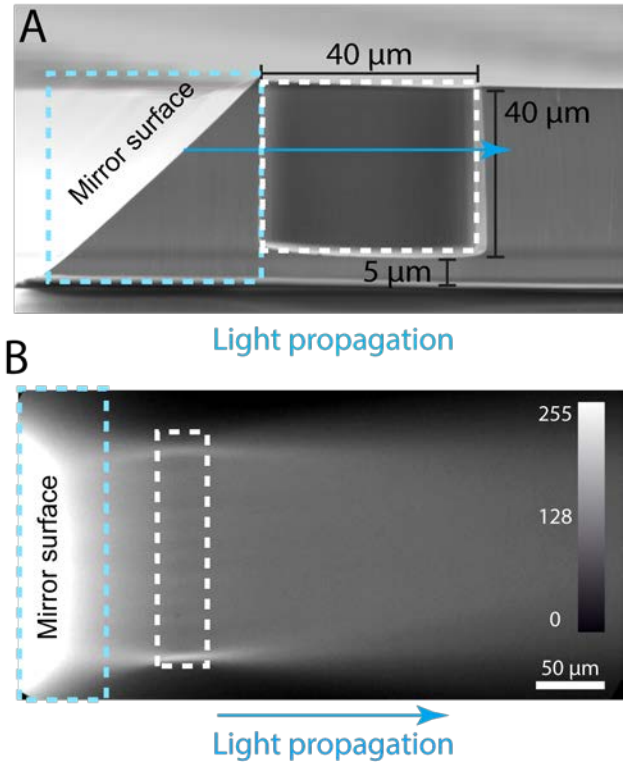

Figure S1: soSPIM light-sheet path. A: Sample mounting micro-well cross section view, the blue dotted region shows the mirror surface and white region shows the position of micro-well with respect to the mirror surface. B: Top view of the light-sheet after reflection on a 45° mirror and imaging through a fluorescent solution.

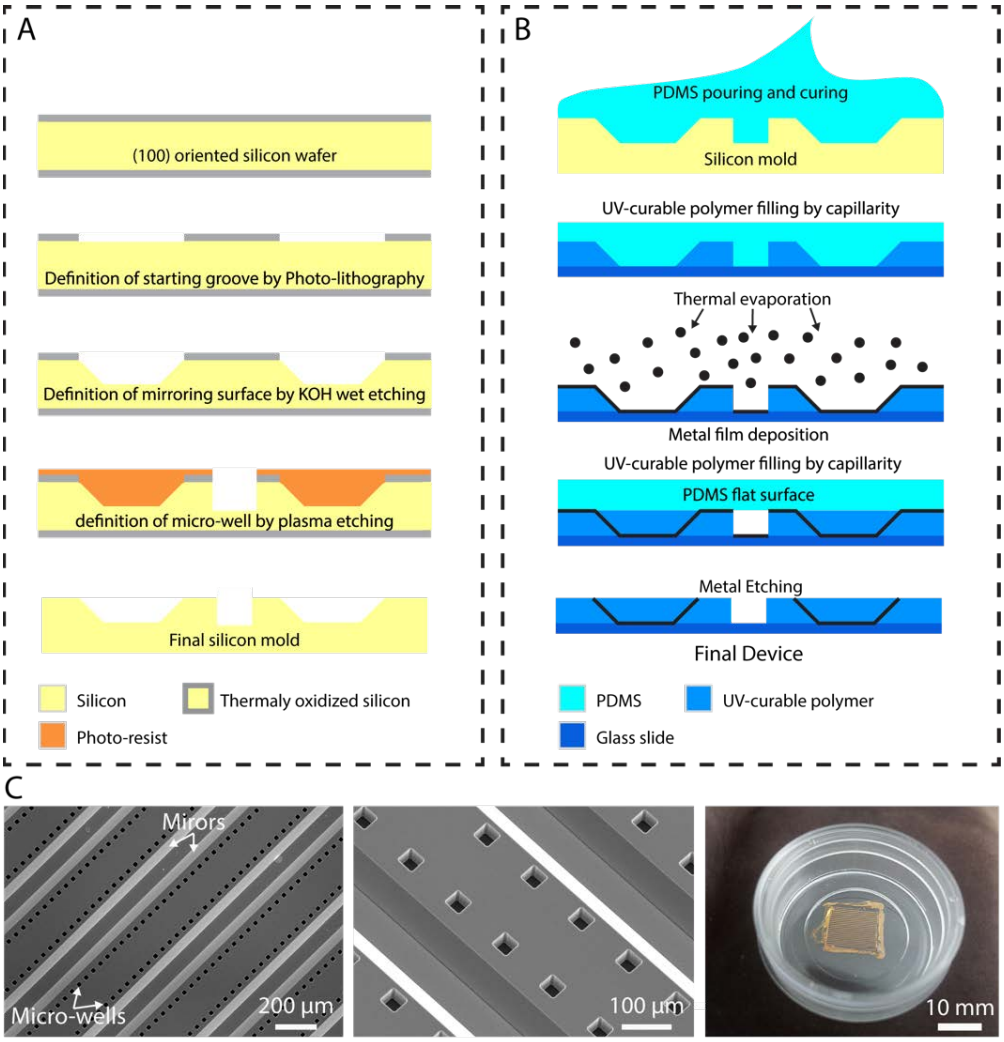

Figure S2: Micro-fabrication process of the device displaying 45° mirrors alongside micro-wells. A: Anisotropic wet etching and dry etching were sequentially used to create 45° surfaces and micro-wells respectively within a silicon wafer. B: Replication of the silicon wafer features onto coverslips and metallization of the 45° surfaces. A PDMS replica of the silicon wafer is created and then used to reproduce the wafer features onto a coverslip in a UV-curable polymer via a capillary filling process. The polymer surface is then coated with a metal layer to make the 45° surfaces reflective. Lastly, the 45° surfaces are protected by an additional layer of UV-curable polymer via a capillary filling process and the unprotected metal removed by wet etching. C: Left and middle panels: SEM images of a silicon wafer displaying 45° surfaces alongside micro-wells. Right panel: Image of a final device produced in a UV-curable polymer and metallized, and sealed on a bottom free plastic dish for easy cell culturing and handling.

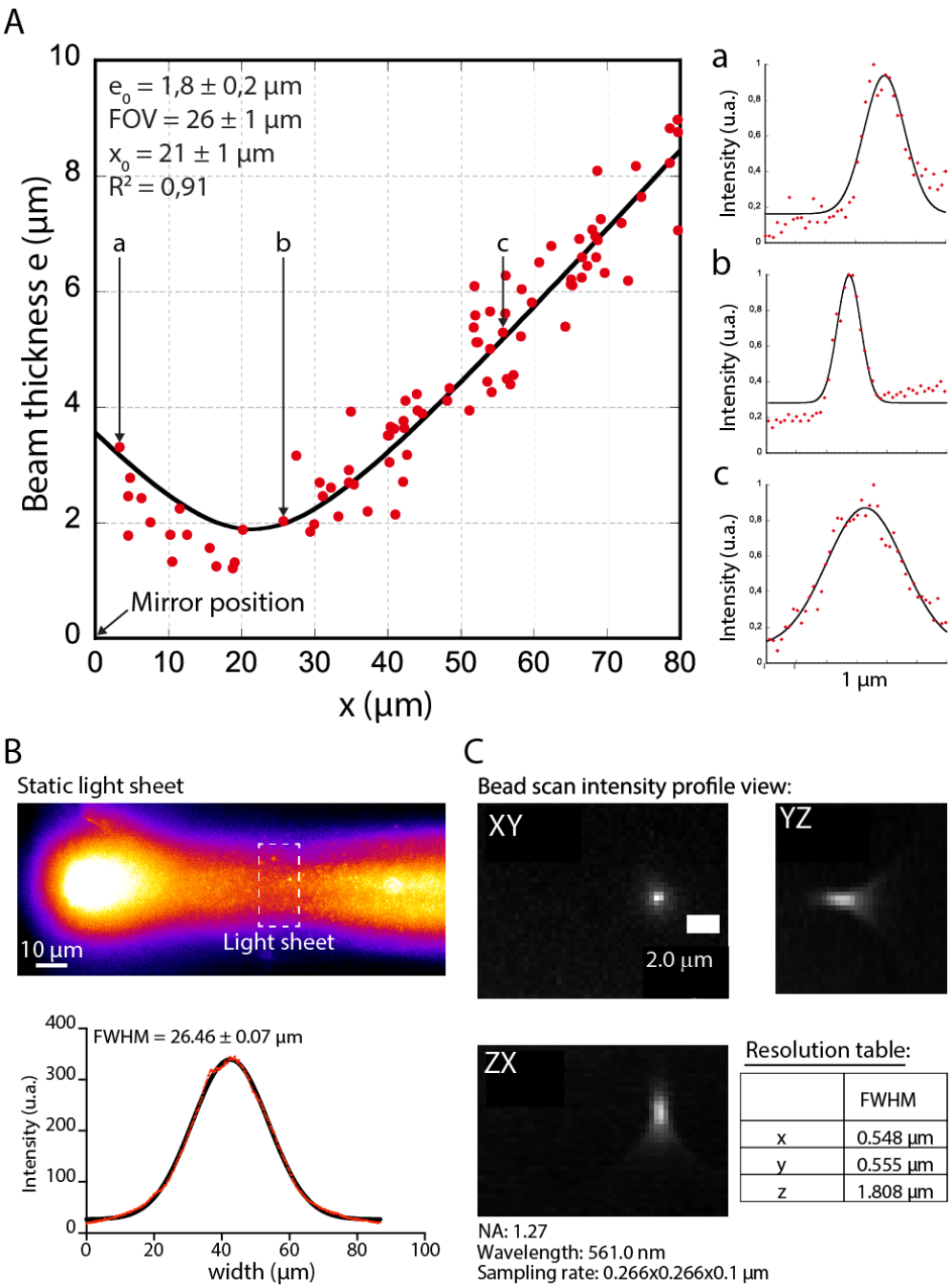

Figure S3: soSPIM light sheet profile characterization and PSF determination. A: Shows the axial dimensions (FWHM) estimated by Gaussian fitting of beads embedded in agar and imaged in the soSPIM configuration according to their position from the mirror (red dots). The black line represents the fit with the Gaussian beam propagation equation (see Methods in main text) and the reported value the result of the fit. The insets (a-c) represent the axial profile of three different beads (red dots) at different positions from the mirror (as highlighted in main panel) and their respective Gaussian fit (black line). B: Top-The light sheet imaged through fluorescent polymer after reflection on a 45° mirror (top Fig. S3). Bottom-

Protein dynamics within 3D cell nucleus

Experimental profile (red dots) and Gaussian fit (black line) of the light-sheet profile averaged on the whit box on top. The reported value is the fit result and represent the estimated static light-sheet width. C: PSF determined by bead scan. 100 nm fluorescent beads were embedded in 1% agarose and imaged on an EMCCD, Evolve512 (pixel size 266 nm), lateral (XY) and axial cross-sectional views (YZ, XZ) are shown. The line intensity was fitted with a Gaussian function and the typical values for lateral PSF are tabulated in the bottom right table.

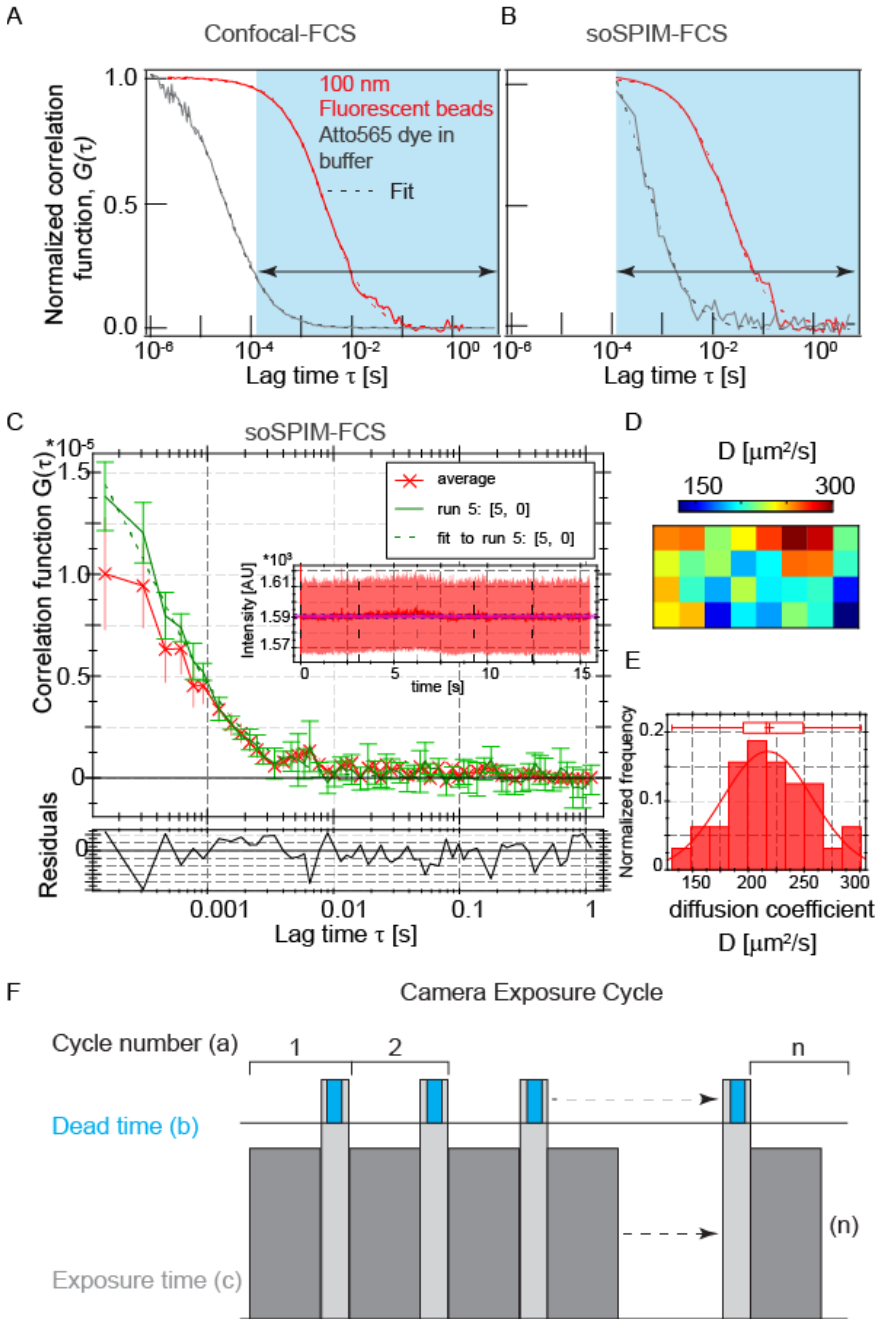

Figure S4: Typical autocorrelation function ACF obtained from Atto565 organic dyes (gray) and 100 nm fluorescent beads (red) in 1xPBS buffer. A-B: ACFs obtained on confocal FCS setup and on soSPIM-FCS setup respectively. Light blue region shows the time scale which can be captured on camera based FCS. Diffusion values obtained are tabulated in Table S3. Note: Due to slow acquisition rate (155 µs) of sCMOS camera diffusion coefficient of organic dyes will be underestimated than the actual value. In

addition, 100 nm fluorescent beads in buffer solution provides a good estimate of absolute diffusion coefficient (see Table S3). C: Autocorrelation function obtained from Atto565 organic dyes in 1xPBS buffer. Red curve shows the ACF from a single pixel and the average ACF for all the data points are shown in green. Inset image shows fluorescence intensity collected over time. D-E: Diffusion maps and histogram are shown. The average D value for Atto 565 dye for all the pixels is 220 ±40 $\mu m^2/s$. soSPIM data were acquired with an sCMOS camera using a 32x32 beads (32x16 organic dyes) pixel ROI at 155 μs camera integration time. Dashed lines correspond to fits of Eq. 2, see Supporting Material. F shows typical camera readout schemes. The pixel size for the analysis was 160 nm and the correlation analysis was performed with 4x4 pixel binning for dye and no binning for 100 nm fluorescent beads.

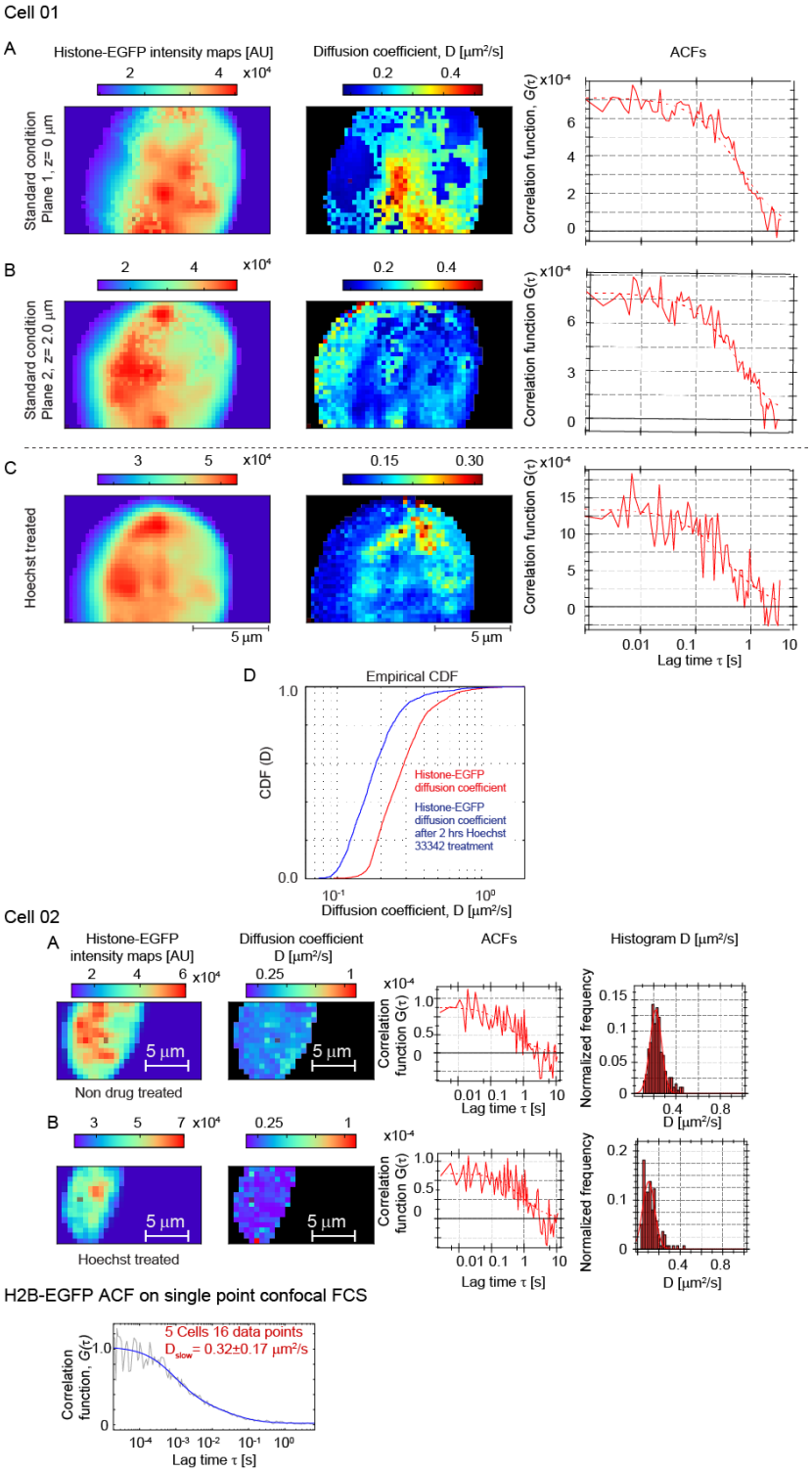

Figure S5: Multi-plane diffusion maps of H2B-eGFP protein in NIH3T3 cells collected on an EMCCD camera. Cell01:- A-B: FCS for two different

z-planes in the cell nucleus. Left - Average fluorescence intensity map for 20k frames; center - diffusion maps; right - typical ACFs. C: As (A) but after DNA binding drug treatment. D: Diffusion coefficient CDF before (red) and after (blue) DNA binding drug treatment. The pixel size for the analysis is 266 nm and the correlation analysis was performed without pixel binning. Cell02:- Similar treatment were performed on cell 2. Histone-EGFP diffusion before (A) and after (B) DNA-binding Hoechst 33342 treatment. Left: fluorescence intensity and diffusion maps. Right: ACFs and corresponding histogram of inferred diffusion coefficients. The pixel size for the analysis is 266 nm and the correlation analysis was performed with 2x2 pixel binning. Bottom figure shows the normalized ACF of Histone-eGFP in live cells at 37 °C on a single point confocal FCS setup.

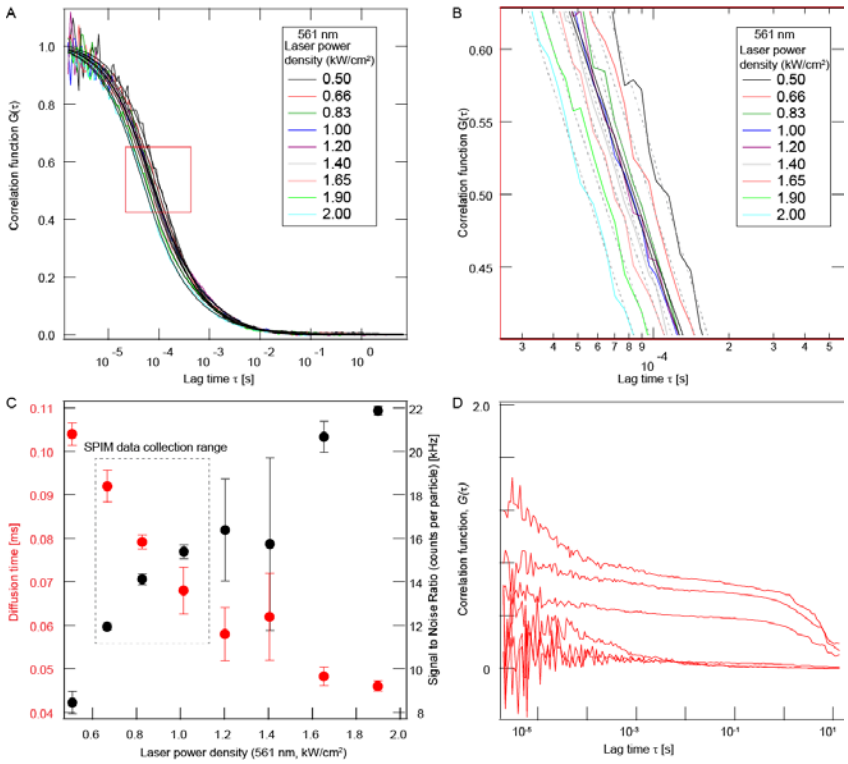

Figure S6: Characterization of 561 and 405 nm laser power dependence on diffusion time of Dendra2 protein. A: Shows ACFs of 3xNLS-Dendra2 ACFs at different 561 nm laser power (at constant 405 nm laser 0.05 kW/cm^2). B: Shows the zoomed red region of A. C: Shows continuous decrease in diffusion time (red left side) and increase counts per particle (black right side). D: Typical correlation function obtained from fixed cells expressing 3xNLS-*Dendra2* on a single point confocal setup.

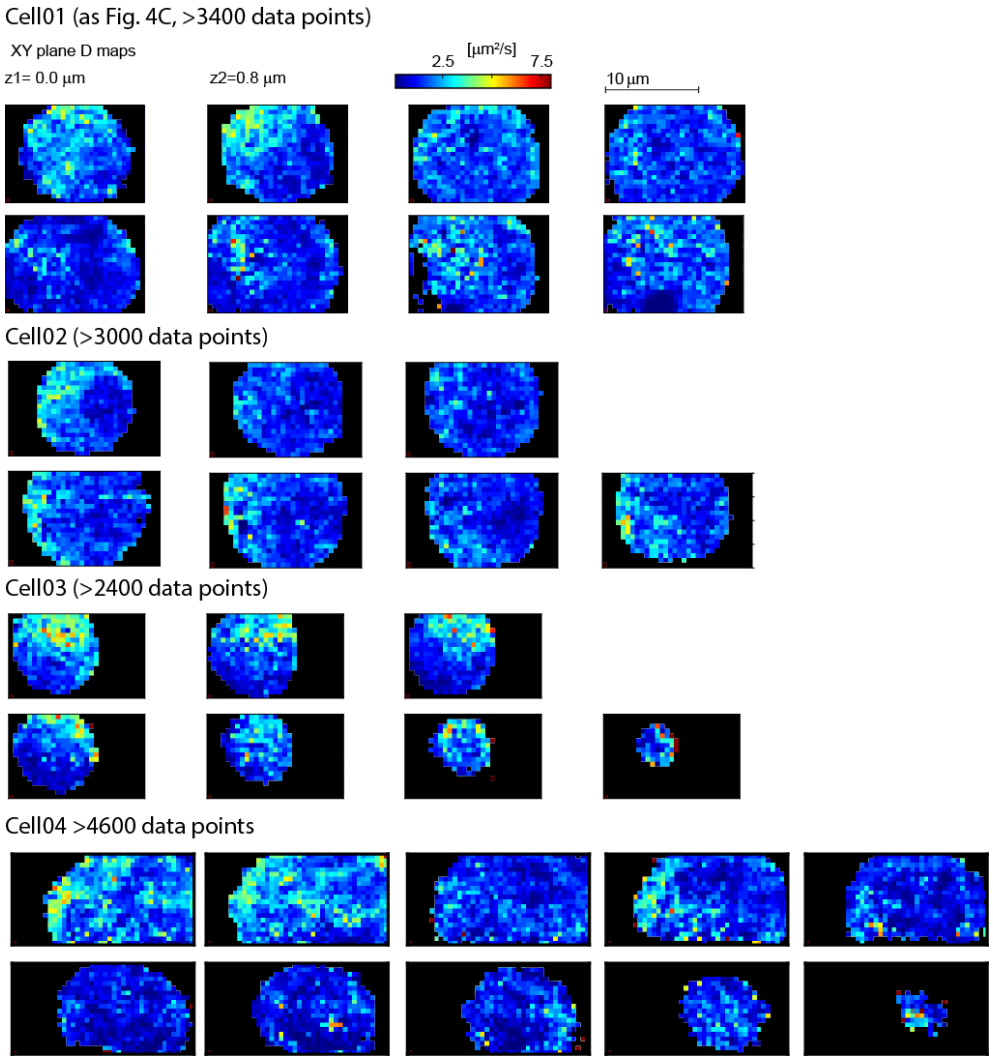

Figure S7: Representative diffusion maps for Dendra2-Pol II cell nucleus at different z-positions. All imaging performed on a sCMOS camera with effective pixel size = 160 nm. ACF analysis was performed with 3x3 pixel binning.

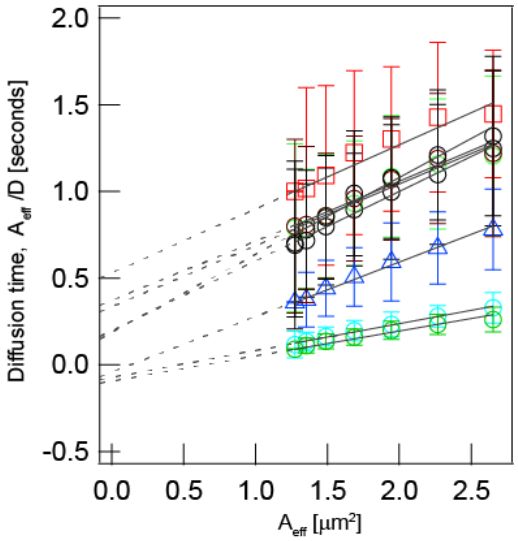

Figure S8: Representative diffusion law plots for Dendra2-Pol II in U2OS cell nucleus at different z-height. Similar to Fig. 5E but showing all planes.

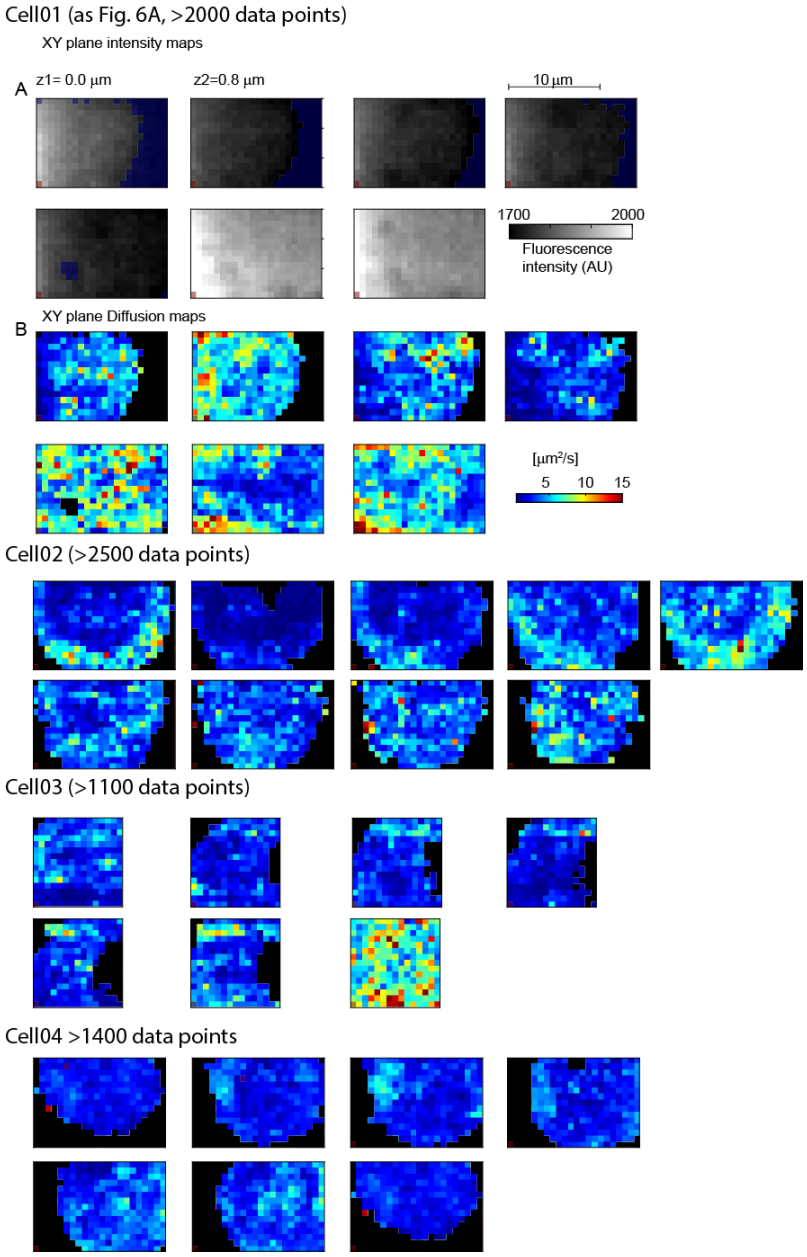

Figure S9: Representative diffusion maps for Dendra2-YAP cell nucleus at different z-positions. All imaging performed on a sCMOS camera with effective pixel size = 160 nm. ACF analysis was performed with 4x4 pixel binning.

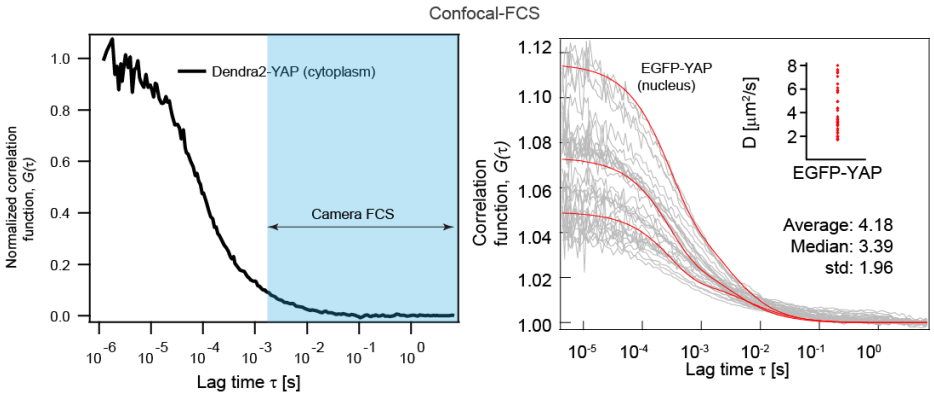

Figure S10: Left- Fast diffusion of Dendra2-YAP in cell cytoplasm performed on a confocal FCS setup at 37°C. Light blue region shows the time scale which can be captured on camera based FCS. Right- Auto-correlation functions obtained with eGFP-YAP on a single point confocal setup (gray curves show all measured profiles and the three red curves are representative fits). Inset: obtained diffusion coefficient value at 37 °C temperature with confocal FCS.

Supplementary Tables

Table S1 Typical camera exposure time and dead time for sCMOS and EMCCD sensors (see Fig. S4).

Type of sensor	Exposure time (ms)	Dead time (ms)
sCMOS Orca-Flash 2.0	0.0380	0.0015
EMCCD512 Evolve	2.00	0.38
EMCCD-iXon3 860 Andor	0.450	0.039

Table S2 Typical soSPIM-FCS data acquisition and post processing settings.

Camera settings	**EMCCD Evolve 512**	**sCMOS ORCA-Flash4.0**
Effective pixel size (μm)	16	6.5
Zoom factor	40-60x	40-60x
Pixel binning		
Data acquisition camera pixel bin	1	1
Postprocessing pixel binning		
• Bright samples (fluorescent beads in buffer)	1	1-3
• Organic dyes in buffer and fluorescent proteins	1-4	3-6
EM-gain	Yes	No EM gain
Bright fluorescent beads in buffer	10-100	NA
Organic dyes in buffer and fluorescent proteins	300	NA
Camera cycle time (ms)		
Organic dyes in buffer	--	0.016-0.160
Fluorescent beads in buffer	2-4	0.016-2.0
Fluorescent proteins in cells	2-5	2-5
Number of frames(k)/time(sec) required		
Organic dyes in buffer	--	60-120/20-40
Fluorescent beads in buffer	20-40/20-40	40-60/20-40
Fluorescent proteins	10-20/30-50	10-20/30-50
Laser Power	**kW/cm^2**	
405 nm laser (photoconversion to red)	0.05-0.2	
561 nm laser (FCS data acquisition)	0.5-1.5	

Table S3 Measured diffusion coefficient value of 100 nm fluorescent beads in 1xPBS (at pH=10) buffer and Histone protein in cell nucleus.

Sample @ °C	**D ($\mu m^2/s$)**	**Method used**	**Refs.**
100 nm Beads			
22 (lab temperature)	*4.80 ±1.80*	*soSPIM-FCS (1024 data points,*	
20 (scaled to 20°C)	*4.53 ±1.69*	*see* **Figure S4***)*	*This study*
25(scaled to 25°C	*5.20 ±1.94*	,,	
37 (scaled to 37°C)	*6.96 ±2.60*	,,	
22 (lab temperature)	*4.18 ±1.76*	,,	
		Confocal FCS (20 data points *see* **Figure S4***)*	
20	4.29	The theoretical diffusion coefficient (Stokes-Einstein relationship)	
20	3.80 ±1.00	SPIM-FCS	(4)
20	3.38 ±0.54	Coherent anti-stokes Raman scattering correlation spectroscopy	(5)
20	4.10 ±0.05	Single point confocal FCS	(4, 6)
21	4.13 ±1.16	3D tracking	(7)
25	4.4 ±0.70	Two focus FCS (2fFCS) and dynamic light scattering (DLS)	(8)
37	6.56 ±0.30	Temporal image correlation spectroscopy (TICS)	(9)
Fluorescent beads T7279	Invitrogen Singapore	100 nm TetraSpec beads	Fluorescent beads T7279
Histone protein in cell nucleus at 37°C			
H2B-EGFP	~0.28	soSPIM-FCS	This study
	~0.32	Confocal FCS	
HP1α-EGFP	0.16-0.4	camera based FCS	Supplementary Table S1. in (10)
Histone *Drosophila* His2Av::mRFP	~0.22	camera based FCS	Figure 9c in ref. (4)
H2A-GFP	~0.22	camera based FCS	See Table 1 in Ref. (4)
Dendra2-H2B	0.5	Single particle tracking	Figure 2—figure supplement 1 in (11)

Table S4 The list of microscope components and materials used in this manuscript.

SN	Name of the component and serial number	Company/ Supplier	Specifications and descriptions
1	Tunable lens Custom EL-30-10	Optotune	focal length from -80 mm to +1000 mm
2	Tube lens AC254-050-A	Thorlabs	focal length 50 mm
3	Galvanometric mirrors SCANMAX	Pangolin SCANMAX 506 actuators	with dielectric Chroma mirrors
4	Nikon Objective Plan Fluor 60x, 1.27 NA	Nikon	High NA objective
5	Telescope lens AC254-150-A	Thorlabs	tube lens of the microscope, focal length 150 mm for both lenses
6	Galvanometric control unit	Pangolin Laser Systems	Laser scanning unit
7	Microscope control software	MetaMorph software	Home written plugins in Visual basic NET
8	UV curable polymer OF-134	MyPolymer	Polymer
9	Pluronic solution F127	Sigma	Surface passivation
10	Fluorescent beads T7279	Invitrogen Singapore	100 nm TetraSpec beads
11	EMCCD 512	Evolve, Princeton Instruments	16 micron pixel size, QE 95 %
12	sCMOS ORCA-Flash4.0 V2	Hamamatsu Japan	6.5 micron pixel size, QE 70%
13	Atto 565 organic dye	Atto-Tech Germany	Carboxy AD 565-21
14	Hoechst 33342	Sigma Singapore	Concentration 0.2 μM for 35 mm culture dish.
15	HEPES buffer solution	Sigma Singapore	10 mM, pH range 6.8-8.2
16	Fetal Bovine Serum F2442	Sigma Singapore	Serum 10%
17	P0781 Penicillin-Streptomycin	Sigma Singapore	1% cell culture media

18	GlutaMAX	10567014 Invitrogen Singapore	1% Cell culture media
19	Agarose	A9414 Sigma Singapore	1.0 % agarose

References

1. Singh, A. P. 2014. Light sheet based fluorescence correlation and cross-correlation spectroscopy for quantitative measurements of bio-molecules in live cells. In Chemistry. National University of Singapore, Singapore.
2. Galland, R., G. Grenci, A. Aravind, V. Viasnoff, V. Studer, and J. B. Sibarita. 2015. 3D high- and super-resolution imaging using single-objective SPIM. Nat Meth 12:641-644.
3. Gaffney, C. J., T. Oka, V. Mazack, D. Hilman, U. Gat, T. Muramatsu, J. Inazawa, A. Golden, D. J. Carey, A. Farooq, G. Tromp, and M. Sudol. 2012. Identification, basic characterization and evolutionary analysis of differentially spliced mRNA isoforms of human YAP1 gene. Gene 509:215-222.
4. Krieger, J. W., A. P. Singh, N. Bag, C. S. Garbe, T. E. Saunders, J. Langowski, and T. Wohland. 2015. Imaging fluorescence (cross-) correlation spectroscopy in live cells and organisms. Nat. Protocols 10:1948-1974.
5. Bailey, K. A., and Z. D. Schultz. 2016. Tracking Bulk and Interfacial Diffusion Using Multiplex Coherent Anti-Stokes Raman Scattering Correlation Spectroscopy. The Journal of Physical Chemistry B 120:6819-6828.
6. Singh, A. P., J. W. Krieger, J. Buchholz, E. Charbon, J. Langowski, and T. Wohland. 2013. The performance of 2D array detectors for light sheet based fluorescence correlation spectroscopy. Opt. Express 21:8652-8668.
7. Perillo, E. P., Y.-L. Liu, K. Huynh, C. Liu, C.-K. Chou, M.-C. Hung, H.-C. Yeh, and A. K. Dunn. 2015. Deep and high-resolution three-dimensional tracking of single particles using nonlinear and multiplexed illumination. Nature communications 6.
8. Müller, C. B., K. Weiß, W. Richtering, A. Loman, and J. Enderlein. 2008. Calibrating Differential Interference Contrast Microscopy with dual-focus Fluorescence Correlation Spectroscopy. Optics express 16:4322-4329.
9. Stasevich, T. J., F. Mueller, A. Michelman-Ribeiro, T. Rosales, J. R. Knutson, and J. G. McNally. Cross-Validating FRAP and FCS to Quantify the Impact of Photobleaching on In Vivo Binding Estimates. Biophysical journal 99:3093-3101.
10. Capoulade, J., M. Wachsmuth, L. Hufnagel, and M. Knop. 2011. Quantitative fluorescence imaging of protein diffusion and interaction in living cells. Nat. Biotechnol 29:835-839.
11. Izeddin, I., V. Récamier, L. Bosanac, I. I. Cissé, L. Boudarene, C. Dugast-Darzacq, F. Proux, O. Bénichou, R. Voituriez, O. Bensaude, M. Dahan, and X. Darzacq. 2014. Single-molecule tracking in live cells reveals distinct target-search strategies of transcription factors in the nucleus. eLife 3:e02230.